Biomed Microdevices
DOI 10.1007/s10544-007-9072-4

Ultraminiature encapsulated accelerometers as a fully implantable sensor for implantable hearing aids

Woo-Tae Park · Kevin N. O'Connor · Kuan-Lin Chen · Joseph R. Mallon Jr. · Toshiki Maetani · Parmita Dalal · Rob N. Candler · Vipin Ayanoor-Vitikkate · Joseph B. Roberson Jr. · Sunil Puria · Thomas W. Kenny

© Springer Science + Business Media, LLC 2007

Abstract Experiments were conducted to evaluate a silicon accelerometer as an implantable sound sensor for implantable hearing aids. The main motivation of this study is to find an alternative sound sensor that is implantable inside the body, yet does not suffer from the signal attenuation from the body. The merit of the accelerometer sensor as a sound sensor will be that it will utilize the natural mechanical conduction in the middle ear as a source of the vibration. With this kind of implantable sound sensor, a totally implantable hearing aid is feasible. A piezoresistive silicon accelerometer that is completely encapsulated with a thin silicon film and long flexible flex-circuit electrical cables were used for this study. The sensor is attached on the middle ear ossicles and measures the vibration transmitted from the tympanic membrane due to the sound in the ear canal. In this study, the sensor is fully characterized on a human cadaveric temporal bone preparation.

Earlier portion of the work in this paper was presented at the 13th International Conference on Solid-State Sensors, Actuators and Microsystems (Transducers) 2005, Seoul Korea.

W.-T. Park (✉) · K.-L. Chen · J. R. Mallon Jr. · P. Dalal · R. N. Candler · V. Ayanoor-Vitikkate · S. Puria · T. W. Kenny
Departments of Mechanical and Electrical Engineering, Stanford University, Stanford, CA 94305, USA
e-mail: wtpark@gmail.com

K. N. O'Connor · T. Maetani · J. B. Roberson Jr. · S. Puria
Department of Otolaryngology—Head and Neck Surgery, Stanford University, Stanford, CA 94305, USA

J. B. Roberson Jr.
California Ear Institute, East Palo Alto, CA, USA

Keywords Accelerometer · Implantable hearing aids · Epi-poly encapsulation · Flex-circuit

1 Introduction

In the United States, although approximately 314 in 1,000 people over age 65 have hearing loss and 40 to 50% of people 75 and older have a hearing loss, only one out of five people who could benefit from a hearing aid actually wears one. This is mainly due to the cost, discomfort, and social stigma for the users. (NIDCD 2005).

There are external hearing aids for people with moderate hearing loss. These consist of a sensor (microphone), conditioning electronics, battery, and a speaker. These simply amplify the sound with a small speaker inside the ear canal. The devices are placed outside the body; in the ear canal or behind the ear. For patients who suffer significant sensorineural hearing loss, there are implantable hearing aids. These devices need to be implanted inside the body to stimulate the inner ear (cochlea). Middle ear hearing aids, which are recently emerging in the market, stimulate the cochlea mechanically. Inner ear hearing aids, also known as cochlear implants, are for patients with severe hearing loss. These devices stimulate the cochlea by means of electrical stimulus. An illustration of a cochlea implant system is shown in Fig. 1. The cochlear implant system consists of the sound sensor (microphone) and the sound processor placed outside the body, implanted circuitry receiving signals from the outer processor wirelessly, and the electrode array that is implanted inside the inner ear (cochlea) to stimulate the auditory nerve cells in each frequency bands. Because of the acoustic impedance of the human tissue, the microphone that is normally used as the sound sensor is required

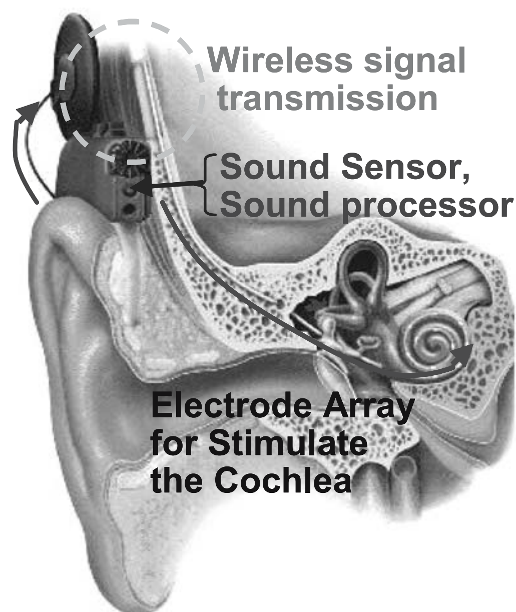

Fig. 1 Illustration of a Cochlear Implant system on a human ear. (MED-EL, Inc.) The sound is picked up externally at the microphone and processed at the sound processor. The processed signal is transmitted across the skin to the implanted part of the system which connects to the electrode array that is inserted inside the inner ear. The electrode stimulates the auditory nerve directly at different locations in the inner ear depending on the frequency of the signal

to be placed outside the body. This requirement limits the implantable hearing aid from being 'fully implantable.' For future hearing aids, there is a great need for totally implantable middle ear and inner ear hearing aids. Zenner et al. (1998) reported an attempt to implant the microphone inside the body by enclosing it inside a titanium canister which is situated beneath the skin of the ear canal. This method is functional but has inherent problems with attenuation and bio-compatibility. There are reports that used a sensor other than a microphone. Most of them are trying to pick up signals from the middle ear anatomy, making use of the mechanical vibrations at the middle ear bones. Many patients with sensorineural hearing deficiency have healthy middle ear ossicles and even patients with conductive hearing deficiency have partially healthy middle ear ossicles that can be completely restored with some simple prostheses.

Puria and Perkins (2003) reported using a 2–3 mm piezoelectric transducer placed in the incudo-stapedial joint (joint between the incus and stapes). Chen et al. (2004) reports a cantilever shape piezoelectric transducer placed at the malleus to pick up the vibrations at the malleus. Chen is reporting the Envoy® system, which is starting to report more clinical trials. Both report a piezoelectric transducer to pick up the vibration. Piezoelectric sensors generate voltage when it is stressed meaning it doesn't need any power source for the sensor element itself. This is considered a merit for designing an implantable hearing aid sensor which should be designed to have low power consumption. Another way of sensing for this application is to use an accelerometer. An accelerometer can be simply attached on one of the middle ear bone and sense the vibration at the site. This method could be simpler in surgical deployment compared to the piezoelectric sensors since part of the sensor does not have to be attached to the surrounding middle ear cavity. The comparison in deployment is shown in Fig. 2. For middle ear implants, any vibration sensor that is deployed at the middle ear will suffer from 'feedback noise' from the mechanical actuation near the oval window. Therefore the middle ear chain needs to undergo a surgery that cuts between the sensing part and the actuation part to separate the sensor from feedback vibration. For cochlear implants, the sensors would be free from 'feedback noise,' since the system uses electrical stimulation.

Accelerometers were heavily used in the biomedical research as a mean to measure vibration and movement in

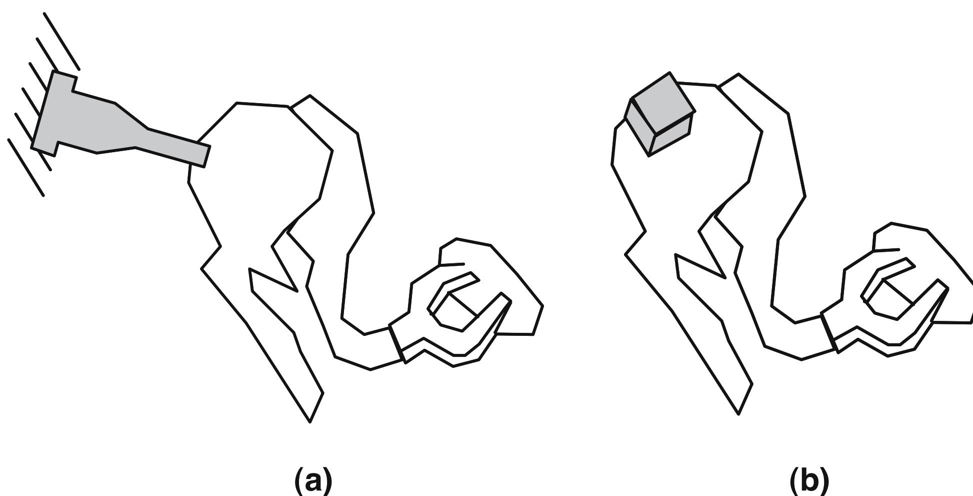

Fig. 2 Illustration of deployment of implantable sensors for hearing aids (electrical connections not shown). (**a**) Representative illustration of a piezoelectric type sensor deployed at the middle ear. The tip of the sensor is attached on the middle ear, and the back end of the sensor has to be attached to the surrounding bone structure of the middle ear cavity. (**b**) Representative illustration of an accelerometer sensor deployed at the middle ear. The sensor is only attached to the middle ear bone

the past (Lowet and Van der Perre 1994; Abrams et al. 1997, 2000; Helman et al. 2000; Keller et al. 2003; Colloca et al. 2003; Pinchak et al. 1981; Evans et al. 1991; Cheng et al. 1995; Fahrenberg et al. 1997; Rostedt et al. 1998; Johansen et al. 2000; Holi and Radhakrishnan 2003; Zou et al. 2004). They were used to measure effects of abdominal vibroacoustic levels at the head of a fetal sheep (Abrams et al. 1997, 2000), the radial epicardial acceleration as a sensor for myocardial function (Helman et al. 2000), or to characterize lumbar spinal manipulation (Keller et al. 2003; Colloca et al. 2003). All of these reports used commercial accelerometers in the millimeter or centimeter dimensions that were the smallest available sensors. The idea of using an accelerometer as a sound sensor for hearing aids was patented by Lesinski and Henderson (1996) in 1996. He reported an idea of using a wafer bonding packaged accelerometer attached to the incus as a sound sensor. Since there were no reports on the performance and no real products following this patent, the feasibility of constructing an accelerometer with conventional wafer bonding packaging, which is small and light enough, yet sensitive enough (resolution) to function as a sound sensor, is questionable. In this work, fully packaged sub-millimeter accelerometers with ultra-thin (38 μm) flexible circuit wiring were developed for ear ossicle movement measurements.

Middle ear ossicular vibration sensor requirements are as follows. First, the weight must be less than a fraction of the attachment point of malleus (20 mg), incus (25 mg), or stapes (3 mg). Secondly, the stiffness of the fine wires must not interfere with the middle ear bone dynamics. Thirdly, it has to have resolution good enough to measure low acceleration at the low frequencies (1 mg at 600 Hz; Aibara et al. 2001). Finally, the bandwidth of the sensor should be large enough to cover the auditory frequency range (0.02 to 20 kHz). The sensor presented in this paper meets many of these requirements.

Size reduction is the main barrier in constructing an accelerometer suitable for measuring middle ear vibrations and the main barrier of size reduction of any MEMS device is the packaging. We have used our wafer-scale epi-poly encapsulation technology to further reduce the size of our packaged accelerometers (Park et al. 2006). Using this method of packaging, we can reduce the area of the package to sub-millimeter dimensions.

This paper will discuss the accelerometer, the flexible circuit packaging, and the test results of the accelerometer on an in-vitro human cadaveric middle ear bone preparation.

2 Fabrication

The accelerometer used in this work is a piezoresistive accelerometer. Piezoresistive transduction is selected in the study because of its low output impedance characteristic, enabling remote amplification without requiring local amplification circuitry. An illustration and cross-section SEM of the accelerometer used in this study is shown in Fig. 3. The proof mass is suspended by a thin flexure suspended on a single anchor. Piezoresistors are implanted on each side of wall of the flexure so that a lateral acceleration will induce differential strain on the two piezoresistors on each side. The accelerometer is packaged at the wafer level with a film encapsulation technique using thick (20 μm) epitaxial silicon as the encapsulation layer

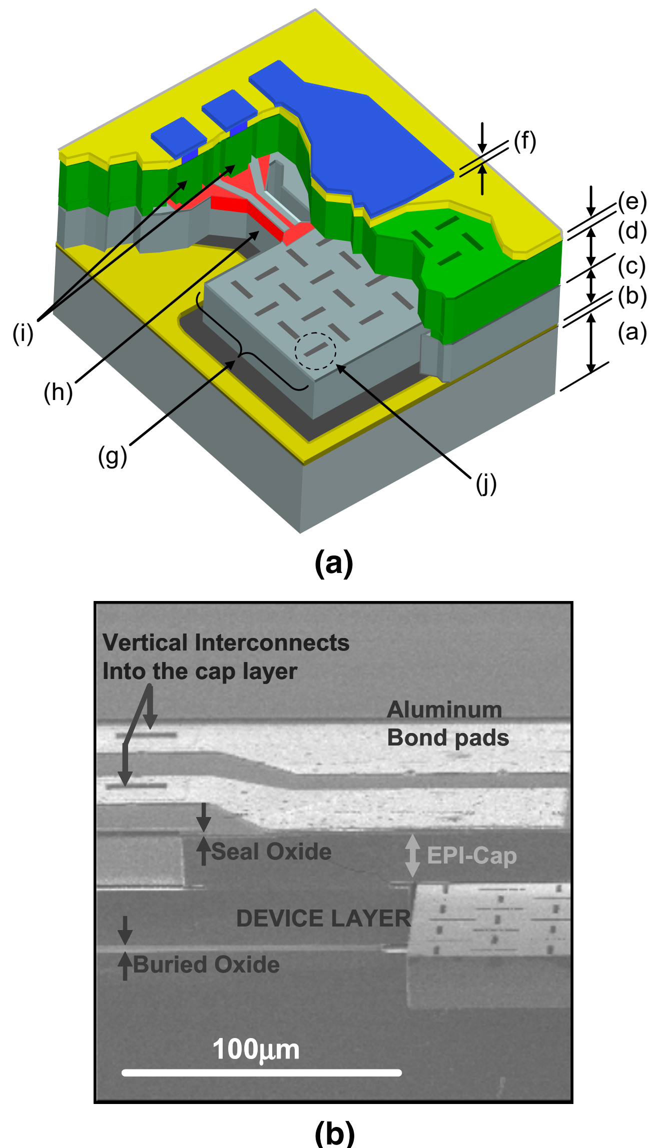

Fig. 3 Sub-millimeter accelerometer. (**a**) Illustration of the of the sensor; (*a*) handle wafer layer, (*b*) buried oxide layer, (*c*) single crystal silicon device layer, (*d*) epitaxially deposited poly silicon encapsulation layer, (*e*) seal LPCVD oxide layer, (*f*) metal layer, (*g*) proof mass, (*h*) flexure with piezoresistors implanted on the sidewall, (*i*) vertical interconnects, (*j*) etch holes for etchant access from top. (**b**) SEM of an intentionally broken sensor to expose inner layers

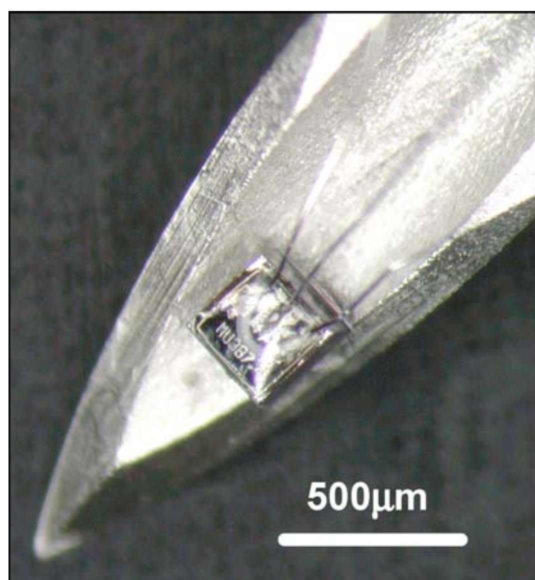

Fig. 4 Photograph of a wired accelerometer in the background of an 18 gauge hypodermic needle. The accelerometer weighs less than 100 μg. Wires are 20 μm in diameter

and LTO (low temperature oxide) for the sacrificial layer that fills the gap between the sensor and the deposited film. The structure is released by vapor-HF and sealed by an LTO film. The signals from the sensor are routed to the top of the package with vertical silicon vias. Metal bond pads are placed on top of the encapsulation. Details of the design and fabrication process can be found in a previous paper (Park et al. 2006).

In order to maximize the sensitivity for a given size of sensor, the flexure width has to be designed as thin as possible. Because of the thermal budget needed for encapsulation, the minimum flexure width was 3 μm. We used TSUPREM4™ to predict the depth of diffusion and verified it with test structures with different flexure widths.

Damping is controlled by the gap size and the gas inside the package. We have control of the gap size in design and the gas pressure inside the package could also be modified by a post process. This post process uses hydrogen to diffuse in and out of the package at an elevated temperature (400°C). Details of this method are covered in another paper (Candler et al. 2005). We can also vent the package in air and reseal the package for critically damped structures.

After the wafer level packaged accelerometers were fully diced, additional packaging was needed to connect the signals from the sub-millimeter diced silicon device to an amplification circuit. The first generation of this “wiring” scheme was to utilize wirebond wires. Figure 4 shows a device with the long aluminum wirebond wire connection on the background of an 18 gauge hypodermic needle. A small amount of epoxy is applied on the wirebond connections to provide additional strength on the bond. Although 5 min epoxy was used, on occasions, the epoxy exerted enough shear stress on the bond connections to tear the bond. This occurs because of its shrinkage during the

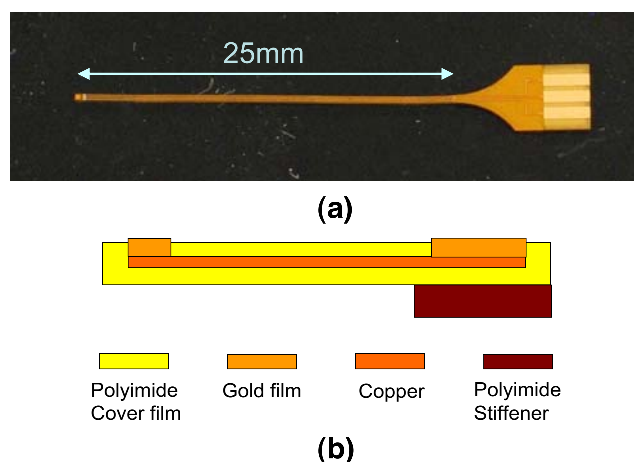

Fig. 5 (**a**) Optical photograph of the topview of the flexible circuit used for the interconnect. (**b**) A schematic of the cross section of the flexible circuit. The material used for the circuit is explained. The figure is not drawn to scale

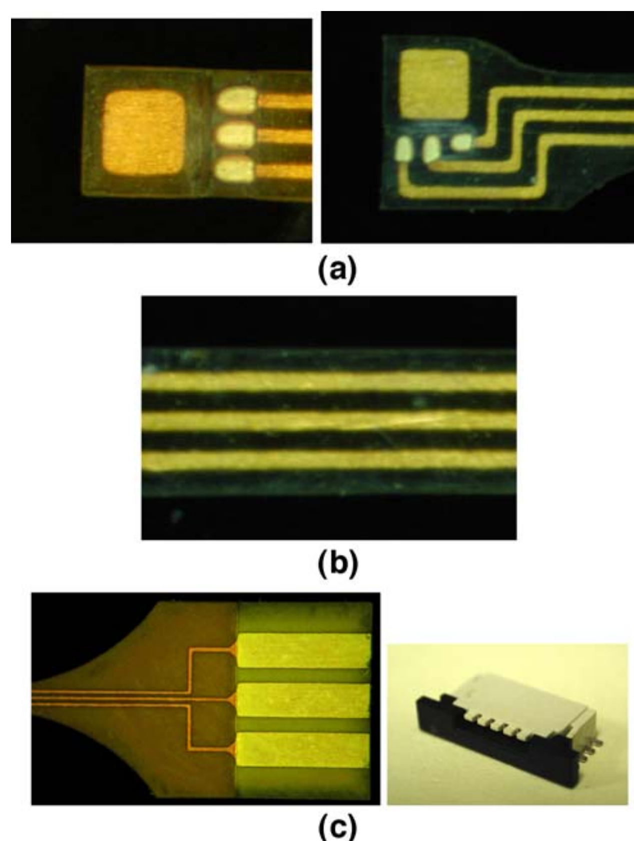

Fig. 6 Close up photographs of different regions of the flexible circuit. (**a**) The left end region is designed to mount the sensor die. (**b**) The copper traces and the spacing are 75 μm wide. (**c**) The right end was designed to be connected to a surface mount connector shown on the right

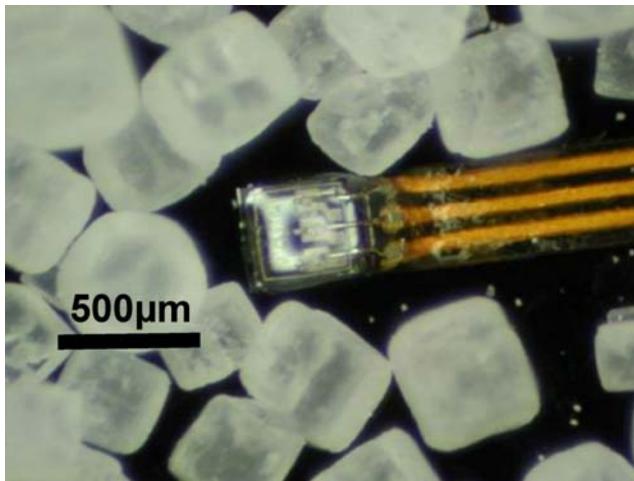

Fig. 7 Optical photograph of a sensor completely packaged on the flexible circuit. A completely packaged sensor is shown in the background of table salt

epoxy curing. An "epoxy glob" is more recommended for this function because of its low shrinkage characteristic. Although this method was functional, the yield was very low (~20%) and the process was very time consuming. Another issue of this type of wiring scheme is that the bare aluminum wire does not have any insulation. Aluminum is prone to build native oxide, Alumina (Al_2O_3), with a thickness of 2–3 nm but this layer can be scraped off easily when the surfaces are in contact with each other. For insulation and possible biocompatibility, a more durable and flexible polymer layer is desired.

In order to overcome the yield loss and poor insulation using the long aluminum wire packaging scheme, a new method of wire packaging was required. Most electronics circuits utilize printed circuit boards. Some of them are on flexible circuit boards. The material used are various polymers; Mylar® (polyester), Kapton® (polyimide), etc. Recently, there are reports of this flexible circuit technology

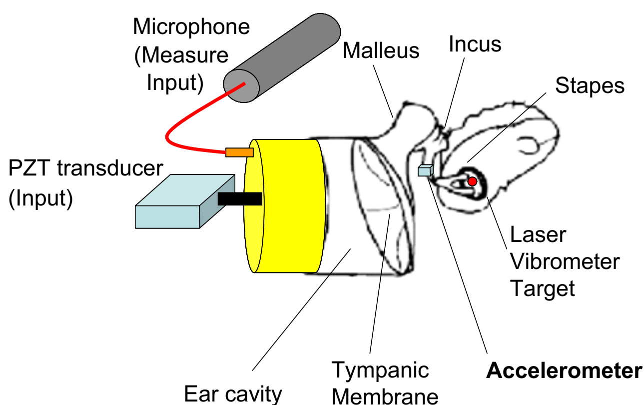

Fig. 8 Measurement setup. The input was measured by a probe-tube microphone. The output was measured at the end of the incus by the accelerometer and the stapes footplate by the laser Doppler vibrometer. There are three sensors in the setup (microphone, accelerometer, and vibrometer)

used for interconnects of ultra-miniature biomedical sensors. Li et al. (2004) patterned a gold deposited layer to form metal traces and contacts on a polyimide suface. The silicon sensor die (commercial pressure sensor) was flip chip bonded on the polyimide package. Although this flexible circuit didn't have any topside insulation layer, it was functional inside a commercial catheter having only the pressure sensor exposed in the ionic solution (blood).

In this work, a copper layer, with a thickness of 13 μm, was used as the metal trace and contacts. The copper traces are sandwiched with two layers of polyimide film (13 μm each) on each side. The total thickness of the flexible circuit is ~38 μm. Each end of the circuit has exposed metal leads with plated gold for connections. On the end which is designed to be connected to a surface mount connector, a 1 mm thick polyimide stiffener is bonded for durable mechanical connection. A topview photograph of the flexible circuit and a schematic of the cross-section are shown in Fig. 5.

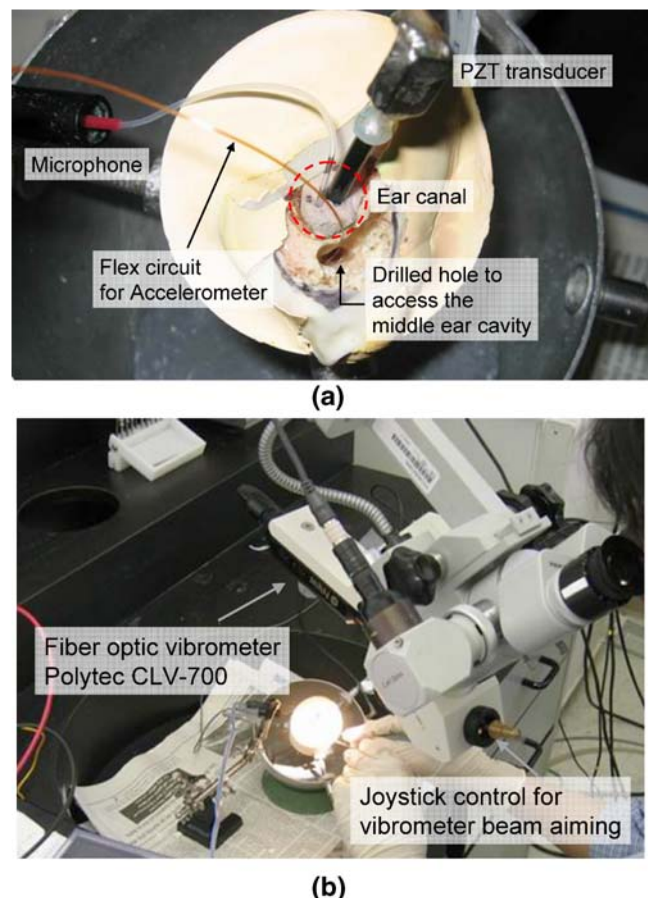

Fig. 9 Photographs of the measurement setup. (**a**) The plastered cadaveric temporal bone sample clamped in fixture with all sensors and actuator installed. (**b**) The fiber optic vibrometer was attached to the microscope. The joystick steers the laser beam to the stapes footplate target. The vibrometer setup was configured specifically for ear mechanics study

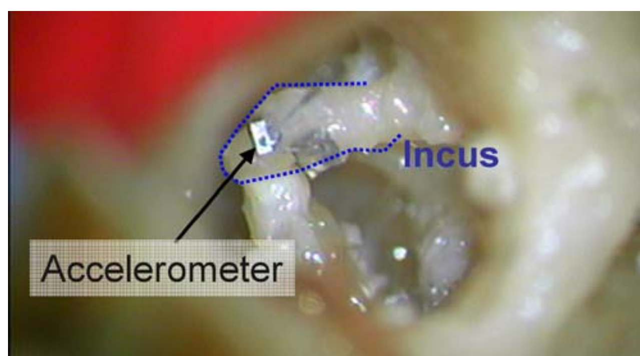

Fig. 10 Close up photograph of the middle ear cavity through the drilled hole on the mastoid. The accelerometer is mounted on the end of the incus. There is another accelerometer is mounted to the right side of it. The second sensor was not used for this study

Details of the flexible circuit are shown in Fig. 6. (a) The left end region was designed to be connected to the sensor silicon die. There are three 75×100 μm gold plated bond pads placed for wirebond placement and there are two different designs to accommodate two different axes in respect to the trace direction. (b) The traces are 75 μm wide and there are 75 μm of spacing between the traces and from the edge of the circuit. There are various lengths of the trace region and they can be selected according to the application the circuit is used for (1″, 2″, and 3″). (c) The right end was designed to be connected to a standard surface mount connector. At the region where the width changes abruptly, the edges are curved to avoid stress concentration and eventual breakage.

The sensors were mounted on the flex circuit by 5 min epoxy. Before the mounting, the polyimide surface is roughened by abrasive paper to prevent the die from peeling off. After the wirebonding, the sensor and metal wirebond were coated with epoxy. Photograph of a sensor completely packaged on the flexible circuit is shown in Fig. 7.

3 Measurement setup

In order to evaluate the accelerometers as a sound sensor, the sensor was tested on a human cadaveric temporal bone sample. There were a total of two bone samples used in this work and the samples were obtained from the Veteran's Hospital at Palo Alto California. The samples were extracted from the cadaver heads with a hole saw. All of the skin was removed and most of the soft tissue was removed. Each bone used in this project was initially frozen and was thawed in a refrigerator for a few days before preparation. Once thawed at room temperature, much of the remaining soft tissue was removed from the sample prior to drilling.

The mastoid, the region behind the ear, was drilled (dental drill) posterior to middle ear cavity (MEC) to expose the stapes footplate and the cochlea. The bone was

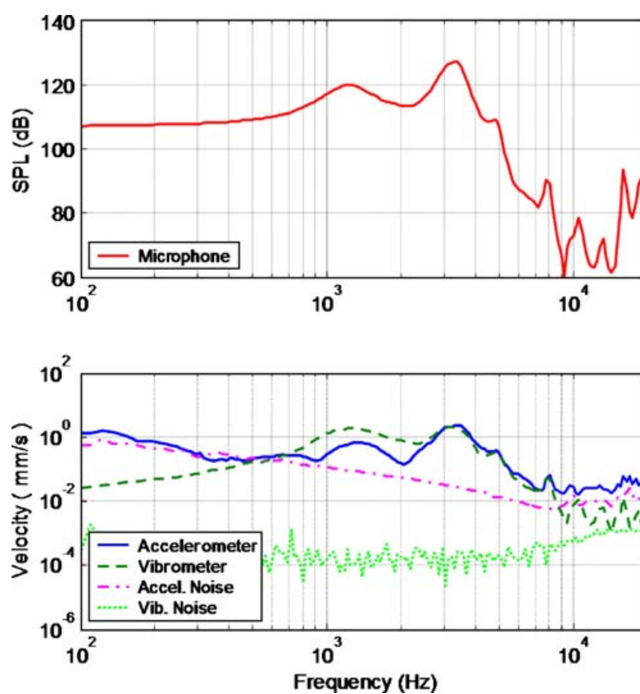

Fig. 11 Results from the first generation device. *Upper plot* shows the SPL at the ear canal measured by the probe-tube microphone near the tympanic membrane. *Lower plot* shows the incus acceleration converted to velocity and the stapes velocity measured by the accelerometer and vibrometer, respectively

then enclosed in two finger cots of a latex examination glove in order to seal in moisture. The covered bone was then placed in a plastic mold, and plaster (KERR Model Stone) was poured into the mold surrounding most of the bone, but leaving the ear canal and the drilled hole to the MEC. Once the plaster hardened, the bone was removed from the mold and the plaster and latex covering the ear canal and middle ear cavity were removed to allow access.

A schematic of the measurement setup using a human cadaveric temporal bone is shown in Fig. 8. A Knowles PZT transducer coupled to the ear canal through a tube

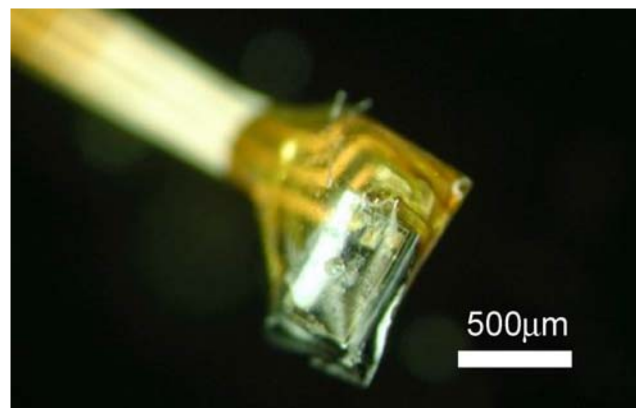

Fig. 12 Close up photograph of the fully packaged accelerometer used for the second measurement

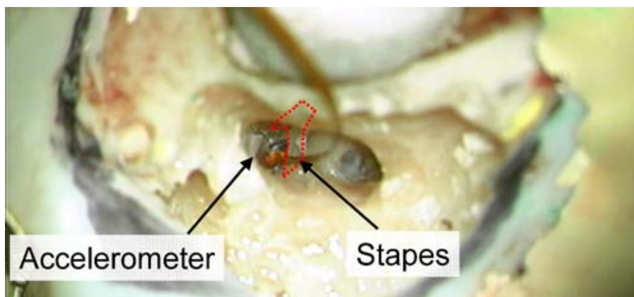

Fig. 13 Photograph of the middle ear cavity through the drilled hole on the mastoid

vibrates the tympanic membrane. This input pressure is measured by a probe-tube microphone (ER-7c, Etymotic Research) within about 3–5 mm distance of the tympanic membrane. The vibration is then conducted to the middle ear bones where the vibration is measured by two sensors. The accelerometer measures the vibration at two locations of the middle ear (incus and stapes) and the laser Doppler vibrometer measures the stapes footplate. A couple of photographs of the measurement setup are shown in Fig. 9.

The reflective target used for the laser Doppler vibrometer is micro glass beads. Since the reflective target (stapes footplate) of the vibrometer is not necessary perpendicular to the incident laser light, a retro reflective material is desired. For the retro reflective material, micro glass beads are used. The glass beads act like prisms, bending the light rays back to the source by refraction.

4 Results

All of the results were taken in the frequency bandwidth of 100 Hz to 20 kHz. The bass bandwidth (20–100 Hz) was ignored since the input PZT transducer does not supply that bandwidth. The microphone signal was converted to sound pressure level. The accelerometer signal was converted to velocity in order to match the vibrometer signal.

The first measurements were taken using a sub-millimeter accelerometer, $387\times387\times230$ μm volume, 80 μg mass, and 4 μm flexure, packaged with long aluminum wirebond wiring. Figure 10 shows a close-up photograph of this accelerometer mounted at the end of the incus.

The ear-canal pressure vs. frequency (input) and the velocity of incus and stapes vs. frequency (output) are plotted in Fig. 11. The results here show the sensor outputs when the PZT transducer was turned on and connected to the tube close to the tympanic membrane. Above about 800 Hz and below 10 kHz, there was general agreement between the accelerometer and LDV velocity measurements. Differences between the two were due to the difference in the measurement angle.

Results at the incus show good agreement for frequencies above 800 Hz and below 10 kHz. However, the input signal was quite high. The amplitude was 100 to 130 dB SPL at the important bandwidth (0.1–5 kHz). This amplitude is equivalent to “very hard rock music” to “jet engine” amplitude which is much higher than conversation speech level (65 dB SPL).

The main reason for such low performance was due to the difference between the noise measurement of the sensor in the laboratory setting and the in-situ noise of the sensor attached in the cadaver preparation. From the noise spectrum of the sensor measured prior to the experiment, we expected a noise floor of 1.64 mg for a resolution bandwidth of 12.2 Hz. However the noise floor in Fig. 11 showed a noise floor over 100 mg for the same bandwidth. Contributing factors are suspected to be the wiring scheme and the attachment technique.

In order to get rid of the influence of the wiring associated noise, the second generation devices were electrically wired with flexible circuits. The sub-millimeter accelerometer, $387\times800\times230$ μm volume, 166 μg mass, and a flexure of 8 μm wide was used for the second measurement. This sensor is six times more sensitive than the sensor used in the previous experiment. The flexible

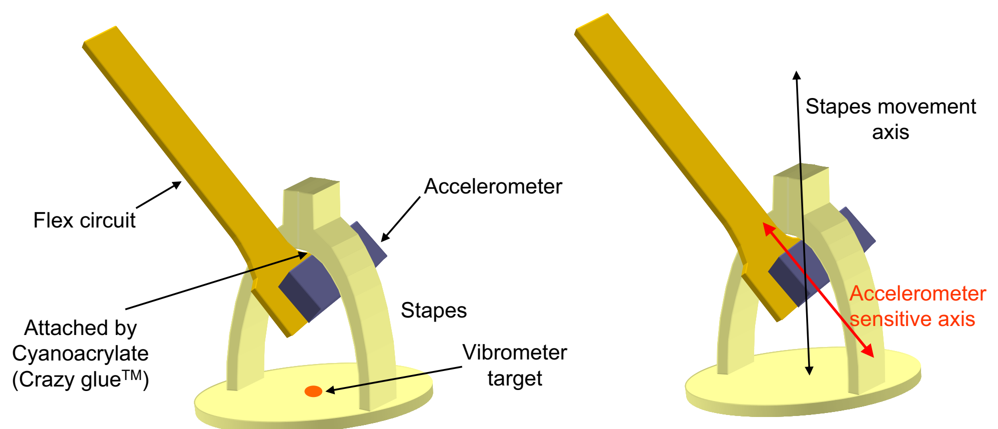

Fig. 14 Close up illustration showing the accelerometer attachment and the vibrometer target. The discrepancy between the measurement angles between the two sensors is compensated when plotting the results

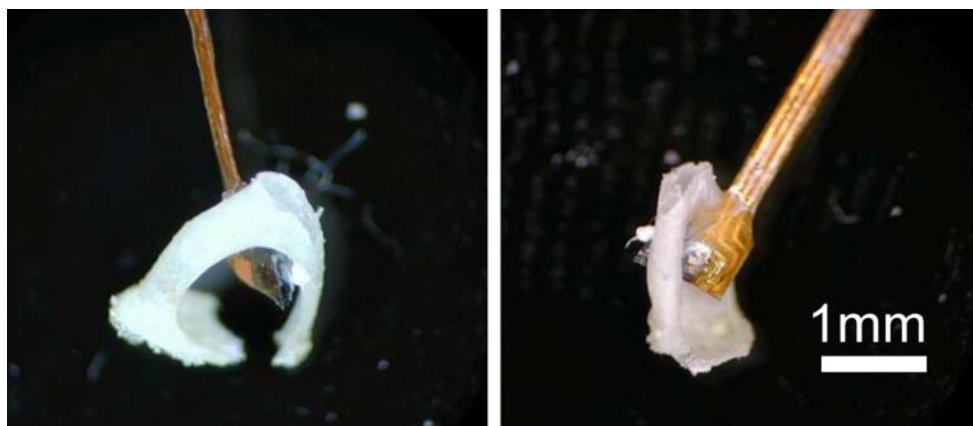

Fig. 15 A close up photograph of the sensor attachment taken after the measurement. It is shown in two angles. The stapes is the smallest bone in a human body

circuit used had an arrangement of connection leads to have the sensitive axis parallel to the copper traces. A Photograph of the accelerometer is shown in Fig. 12.

Figures 13–17 shows close up photographs and illustration of accelerometer deployed in the middle ear cavity. Figure 13 shows the accelerometer attached to the stapes. Figure 14 shows a close up illustration showing the attachment. Figure 15 shows real photographs of this close up taken after the experiment. Figure 16 shows a photograph of the incudo-stapedial joint accidentally fused with cyanoacrylate (Crazy glue™). Figure 17 shows the incudo-stapedial joint intentionally detached in order to investigate the acoustic coupling between the tympanic membrane and the cochlea.

Before evaluating the accelerometer as a sound sensor, the flexible circuit needs to be tested to see if it exerts any stiffness to the middle ear ossicular chain dynamics. For this test, the vibrometer sensor measures the stapes velocity before and after the accelerometer and flexible circuit installation on the stapes. In Fig. 18, one can see only a little difference in the low frequency bandwidth (100–700 Hz) and no difference in the rest of the frequency bandwidth. Therefore, one can conclude that the flexible circuit exerts very little, if any, stiffness to the middle ear ossicular chain dynamics.

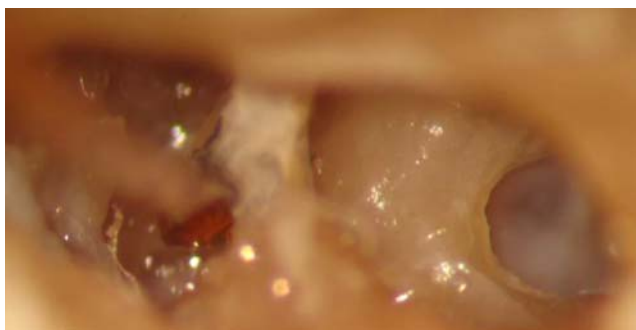

Fig. 16 A photograph of the incudo-stapedial joint accidentally fused with cyanoacrylate (Crazy glue™). Much attention is required during the sensor attachment with glue

The noise floor of the microphone, the accelerometer, and the vibrometer were measured to obtain the resolution of each sensor (Fig. 19). The PZT transducer was turned off and all three sensors were used for measuring the voltage output at the audible frequency bandwidth (0.1–20 kHz). Since there are only two inputs for the data acquisition board for this setup, the accelerometer and the vibrometer signal were measured separately. The microphone noise seems to be more consistent in all bandwidth compared to the first measurements. What was noticeable is that the noise floor of the accelerometer is two orders of magnitude lower compared to the first measurements. This is due to more sensitivity (×6) of the accelerometer and lower noise of the flexible circuit packaging.

The first stapes velocity measurement was collected with the incudo-stapedial joint (joint between incus and stapes) fused accidentally (Fig. 20). This reduces the vibration conduction in the middle ear ossicles. The reduction is noticeable compared to the next results without fusing of the joint (Fig. 21). In order to create different sound levels, the PZT transducer's intensity varied from 1 mV to 250 mV. The corresponding sound level (SPL) was from 60 (conversation) to 120 dB (jet engine). The results show stapes velocity follows the input very well unless it is limited by the accelerometer noise floor. At the lowest input (60–70 dB), the accelerometer can only detect signals in the bandwidth of 2 to 10 kHz.

Fig. 17 A photograph of incudo-stapedial joint intentionally detached in order to investigate the acoustic coupling between the tympanic membrane and the cochlea

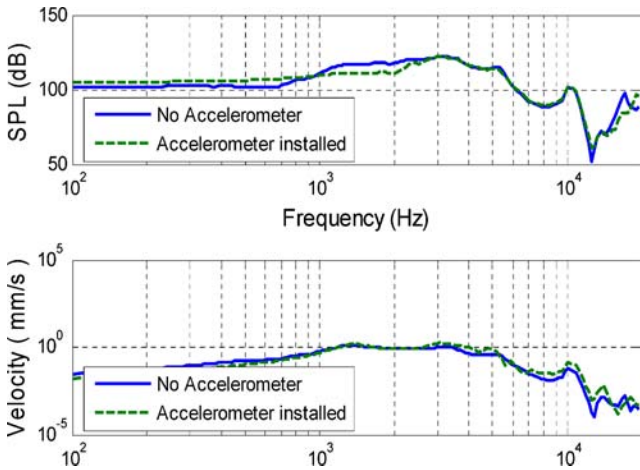

Fig. 18 Comparison of the stapes velocity before and after accelerometer installation. There is very small stapes velocity difference between the two situations. Input (microphone) shown on *upper side* and output (accelerometer) shown on *lower side*

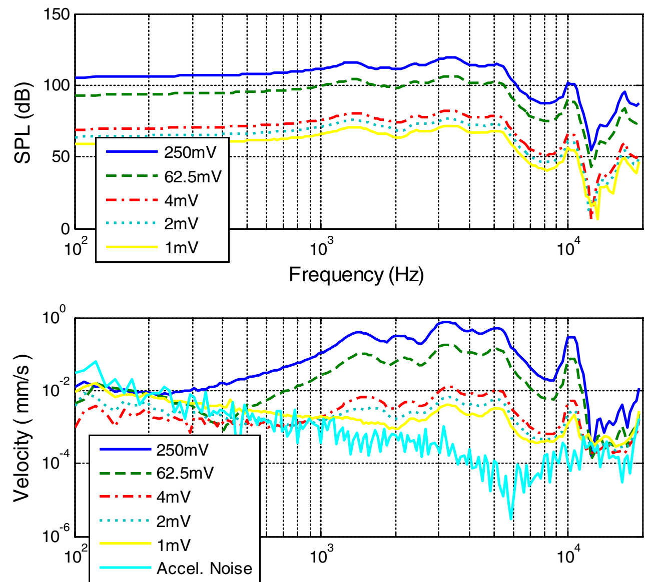

Fig. 20 Stapes velocity (*lower plot*) measured by accelerometer plotted with the varying input sound pressure level (*upper plot*). The accelerometer follows the input well except the regions limited by the noise floor

The stapes velocity was measured for a second time with the epoxy on the incudo-stapedial joint removed (Fig. 21). The response improvement was noticeable compared to the previous plot (Fig. 20). Since the signal to noise ratio was larger than the previous result, the detectable frequency bandwidth is wider (900 Hz to 10 kHz) for the lowest input of 1 mV (55 to 75 dB SPL). Because the sensor used had the primary resonance peak at 6 kHz, the noise equivalent velocity had a "dip" at 6 kHz and noise increase over 6 kHz because the sensitivity drops.

To confirm the accelerometer output, the vibrometer was again used to measure the vibration in a close location (refer to Fig. 14). The comparison of the output of the two sensors is plotted in Fig. 22.

The output was compared with the two extreme input levels (1 and 250 mV) of this experiment. At the highest input (250 mV), both sensors were not limited by noise.

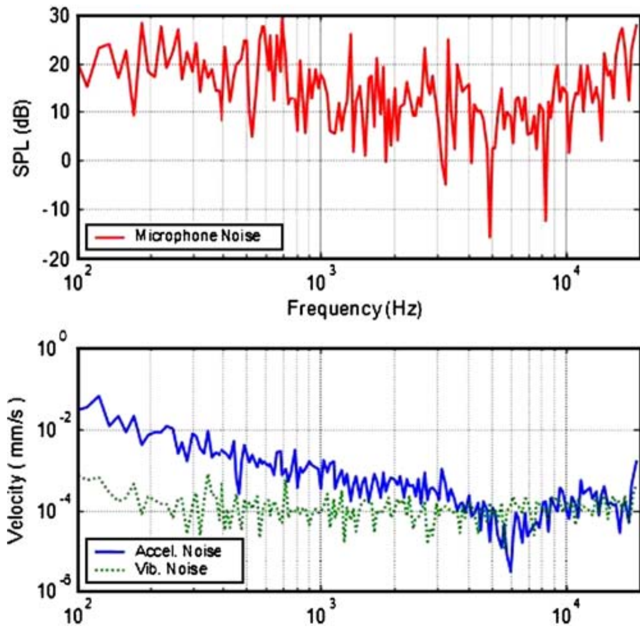

Fig. 19 Noise floor of all sensors for the second measurement. The accelerometer and the vibrometer noise are expressed in velocity. Notice the two orders of magnitude lower accelerometer noise compared to the previous measurement (Fig. 11)

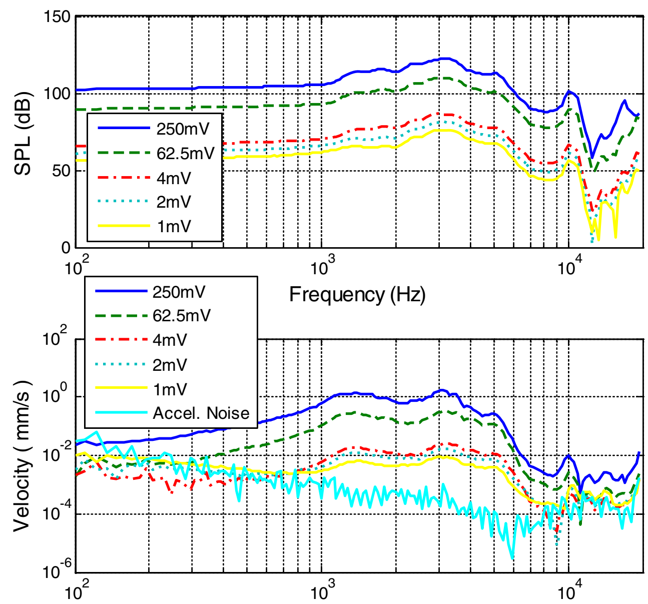

Fig. 21 Stapes velocity (*lower plot*) measured by accelerometer plotted with the varying input sound pressure level (*upper plot*). The icudo-stapedial joint is released which increased accelerometer response amplitude

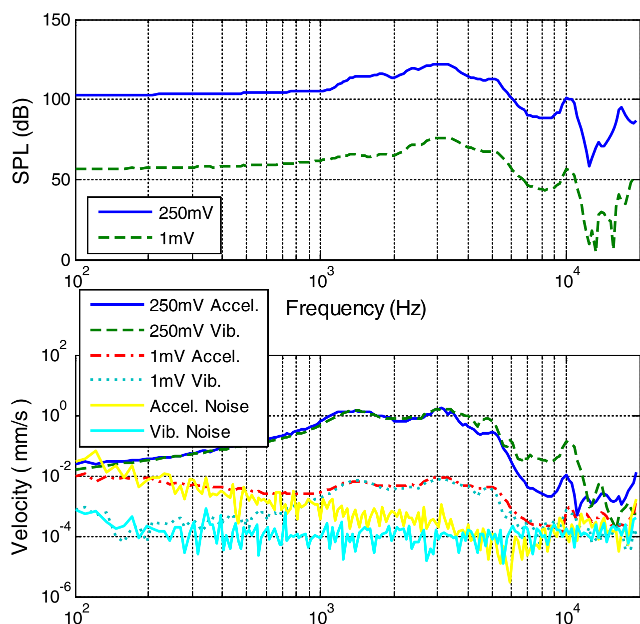

Fig. 22 Comparison of the outputs of two sensors, the accelerometer and the laser vibrometer. The output (*lower plot*) was compared at the highest and the lowest input (*upper plot*). The signal to noise ratio of the accelerometer is comparable to the vibrometer

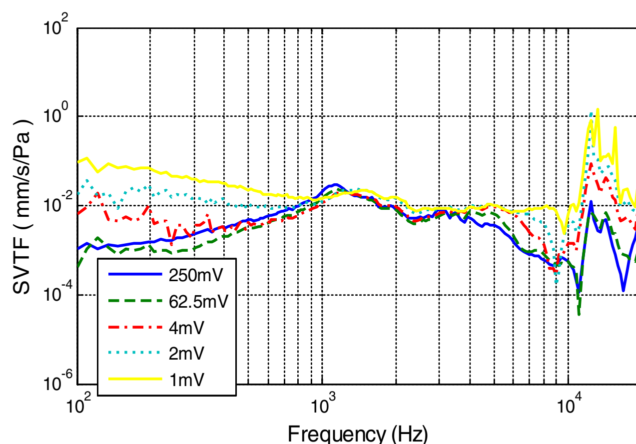

Fig. 23 Stapes footplate velocity transfer function at different input amplitudes. The accelerometer response linearity can be confirmed with this plot

The discrepancy between the two sensors above 6 kHz is suspected to be due to measurement axis difference. At the lowest input (1 mV), both sensors were limited by noise in certain bandwidths. The vibrometer sensor has slightly lower detectable frequency bandwidth (800 Hz–6 kHz) than the accelerometer sensor's frequency bandwidth (1–8 kHz). The signal to noise ratio of the accelerometer was comparable to the laser vibrometer sensor above 1 kHz. Even though this is a remarkable result, the performance (signal to noise ratio) still has to be improved to replace the conventional microphone. While loud conversational speech has a level of 65 dB SPL, the accelerometer noise should ideally be limited to an equivalent of 25–30 dB, 40 dB less than the signal level output of 1 mV.

The performance of the system can be improved by two factors; improved the accelerometer performance and higher vibration signal at the accelerometer deployment site. The accelerometer's performance is limited by the sensor's sensitivity, accelerometer noise, and the amplifier noise. Improvements in all of these factors can contribute to a higher performance sensor.

In order to increase the vibration, the accelerometer can be mounted on different middle ear bones; the malleus or the incus. This should theoretically increase the signal. Another arrangement would be attaching the accelerometer at the end of the incus and removing the stapes. This might also increase the vibration. The reason the stapes was selected for the attachment site for this measurement was because it has the advantage of high mechanical impedance (the accelerometer does not load the ossicles dynamics, as demonstrated earlier in Fig. 18). The mechanical impedance of the sensor should be demonstrated with each different sensor attachments.

Figure 23 is showing the transfer function of the middle ear ossicles measured by the accelerometers. The stapes footplate velocity transfer function is defined by

$$\mathrm{SVTF} = \frac{\text{velocity}\ [\text{mm/s}](\text{from Accelerometer})}{\text{pressure}\ [\text{Pa}](\text{from Microphone})}$$

Among the information this plot can provide, it shows the linearity of the accelerometer as a sound sensor.

In order to investigate the acoustic coupling between the tympanic membrane and the cochlea, the ISJ

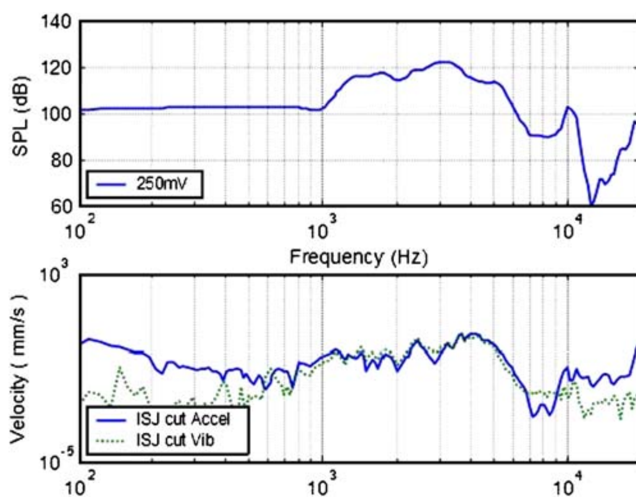

Fig. 24 Acoustic coupling between the tympanic membrane and the cochlea. *Upper plot* shows the input measured at the ear canal, and *low plot* shows the corresponding accelerometer & vibrometer signal at the cochlea with incudo-stapedial joint cut

(icudo-stapedial joint) was intentionally removed for this experiment. With the ISJ removed and the PZT transducer at the highest input level, the response of the stapes, representing the movement of the oval window of the cochlea, was measured by the two sensors. From Fig. 24, one can see only a slight acoustic coupling in the 900 Hz to 7 kHz bandwidth. Acoustic coupling is insignificant because middle ear cavity is open for the experiment.

5 Conclusions and ongoing work

We have successfully demonstrated the feasibility of using an ultra-miniature packaged accelerometer as an alternative sensor for cochlear implants and implantable hearing aids. The sensor can be attached to the middle ear with wires running through the middle ear cavity and to the processor site. Compared to the first generation device results (Fig. 11), there has been great improvement in the device performance (Fig. 22). The accelerometer can measure down to 60 dB SPL at 1 kHz. Since typical externally worn microphones go down to 30 dB SPL (Knowles Electronics®), there still is a lot of room for improvement (~×30). Deployment at a different site in the middle ear can be one method of improvement. So far in this work, measurements at the incus and the stapes have been explored. The malleus is known to have at best three times higher vibrations than the stapes (Puria, private conversations, 2005).

There are also concerns for commercialization of the device. Not all of materials used in this study qualify for biocompatibility as an implantable hearing aid. The long term biocompatibility and reliability of the materials used for the sensor should be explored and characterized. Although piezoresistive transduction is advantageous because of its remote amplification capability, power consumption, which is inherently high for piezoresistors (~mW), is a problem for implantable devices. Other transduction methods such as capacitive, if the required ASIC can be integrated on the encapsulation or piezoelectric, if piezoelectric accelerometers can be manufactured to be small enough, could be also promising as an implantable MEMS accelerometer for hearing aid sensors in the future.

Acknowledgements This work was supported by DARPA HERMIT (ONR N66001-03-1-8942), Bosch Palo Alto Research and Technology Center, a CIS Seed Grant, The National Nanofabrication Users Network facilities funded by the National Science Foundation under award ECS-9731294, and The National Science Foundation Instrumentation for Materials Research Program (DMR 9504099). The authors would especially like to thank Gary Yama[1], Markus Lutz[2], and Aaron Partridge[2] for their guidance and assistance in the device design and fabrication ([1]Robert Bosch Corporation, [2]Robert Bosch Corporation, currently at SiTime).

References

R.M. Abrams, A.J.M. Peters, K.J. Gerhardt, Obstet. Gynecol. **90**, 216 (1997)

R.M. Abrams, A.J.M. Peters, X. Huang, D.E. Wasserman, K.J. Gerhardt, J. Sound Vib. **230**, 725 (2000)

R. Aibara, J.T. Welsh, S. Puria, R.L. Goode, Hear. Res. **152**, 100 (2001)

R.N. Candler, W.-T. Park, M.A. Hopcroft, B. Kim, T.W. Kenny, in *Proceedings of The 13th International Conference on Solid-State Sensors, Actuators and Microsystems (Transducers '05), vol. 2*, Seoul, Korea, 2005, p. 920

D.A. Chen, D.D. Backous, M.A. Arriaga, R. Garvin, D. Kobylek, T. Littman, S. Walgren, D. Lura, Otolaryngol. Head Neck. Surg. **131**, 904 (2004)

S.L. Cheng, J. Timonen, H. Suominen, J. Biomech. **28**, 471 (1995)

C.J. Colloca, T.S. Keller, R. Gunzburg, J. Manip. Physiol. Ther. **26**, 579 (2003)

A.L. Evans, G. Duncan, W. Gilchrist, Med. Biol. Eng. Comput. **29**, 102 (1991)

J. Fahrenberg, F. Foerster, M. Smeja, W. Muller, Psychophysiology **34**, 607 (1997)

D.N. Helman, A.F. Choudhri, D.L.S. Morales, M.R. Williams, M.C. Oz, ASAIO J. **46**, 156 (2000)

M.S. Holi, S. Radhakrishnan, in *IEEE Region 10 Annual International Conference, Proceedings/TENCON, vol. 4*, Bangalore, India, 2003, p. 1395

P. Johansen, C. Riis, J.M. Hasenkam, P.K. Paulsen, H. Nygaard, Proc. Inst. Mech. Eng., H J. Eng. Med. **214**, 121 (2000)

T.S. Keller, C.J. Colloca, R. Gunzburg, J. Manip. Physiol. Ther. **26**, 567 (2003)

S.G. Lesinski, T. Henderson, US Patent 5531787 (1996)

C. Li, F.E. Sauser, R. Azizkhan, C.H. Ahn, I. Papautsky, Tech. Digest, IEEE MEMS, 749 (2004)

G. Lowet, G. Van der Perre, Proc. SPIE Int. Soc. Opt. Eng. **2361**, 305 (1994)

NIDCD, *Statistics about Hearing Disorders, Ear Infections, and Deafness* (National Institutes of Health, Bethesda, MD, 2005)

W.-T. Park, A. Partridge, R.N. Candler, V. Ayanoor-Vitikkate, G. Yama, M. Lutz, T.W. Kenny, Microelectromechanical Syst. **15**, 507 (2006)

A.C. Pinchak, R.S. Wiley, C. Kovijanic, J. Biomech. Eng. **103**, 160 (1981)

S. Puria, R.C. Perkins, US Patent 6554761 (2003)

M. Rostedt, L. Ekstrom, H. Broman, T. Hansson, J. Biomech. **31**, 503 (1998)

H.P. Zenner, M.M. Maassen, P.K. Plinkert, R. Zimmermann, J.W. Baumann, G. Reischl, H. Leysieffer, HNO **46**, 844 (1998)

Q. Zou, W. Tan, E.S. Kim, J. Singh, G.E. Loeb, in *Annual International Conference of the IEEE Engineering in Medicine and Biology—Proceedings, vol. 26*, San Francisco, 2004, p. 4279